Chapter 19
Positive Electrodes in Other Aqueous Systems

19.1 Introduction

This chapter discusses three topics relating to positive electrodes in aqueous electrolyte battery systems, the manganese dioxide electrode, the nickel electrode and the so-called *memory effect* that is found in batteries that have "nickel" positive electrodes.

The first of these deals with a very common material, MnO_2, that is used in the familiar "alkaline" cells that are found in a very large number of small portable electronic devices. This electrode operates by a simple proton insertion reaction.

MnO_2 can have a number of different crystal structures, and it has been known for many years that they exhibit very different electrochemical behavior. It is now recognized that the properties of the most useful version can be explained by the presence of excess protons in the structure, whose charge compensates for that of the Mn^{4+} cation vacancies that result from the electrolytic synthesis method.

The "nickel" electrode is discussed in the following section. This electrode is also ubiquitous, as it is used in several types of common batteries. Actually, this electrode is not metallic nickel at all, but a two-phase mixture of nickel hydroxide and nickel oxy-hydroxide. It is reversible, and also operates by the insertion and deletion of protons. The mechanism involves proton transport through one of the phases that acts as a solid electrolyte. The result is the translation of a two-phase interface at essentially constant potential.

The third topic in this group is a discussion of what has been a vexing problem for consumers. It occurs in batteries that have nickel positive electrodes. The mechanism that results in the appearance of this problem is now understood. In addition, the reason for the success of the commonly used solution to it can be understood.

R.A. Huggins, *Energy Storage*, DOI 10.1007/978-3-319-21239-5_19

19.2 Manganese Dioxide Electrodes in Aqueous Systems

19.2.1 Introduction

Manganese dioxide, MnO_2, is the reactant that is used on the positive side of the very common *alkaline* cells that have zinc as the negative electrode material. There are several versions of MnO_2, some of which are much better for this purpose than others. Thus this matter is more complicated than it might seem at first.

MnO_2 is polymorphic, with several different crystal structures. The form found in mineral deposits has the rutile (beta) structure, and is called *pyrolusite*. It is relatively inactive as a positive electrode reactant in KOH electrolytes. It can be given various chemical treatments to make it more reactive, however. One of these produces a modification containing some additional cations that is called *birnessite*. Manganese dioxide can also be produced chemically, and then generally has the delta structure. The material that is currently much more widely used in batteries is produced electrolytically, and is called *EMD*. It has the gamma (*ramsdellite*) structure.

The reason for the differences in the electrochemical behavior of the several morphological forms of manganese dioxide presented a quandary for a number of years. It was known, however, that the electrochemically active materials contain about 4 % water in their structures that can be removed by heating to elevated temperatures (100–400 °C), but the location and form of that water remained a mystery. This problem was solved by Ruetschi, who introduced a cation vacancy model for MnO_2 [1, 2].

The basic crystal structure of the various forms of MnO_2 contains Mn^{4+} ions in octahedral holes within hexagonally (almost) close packed layers of oxide ions. That means that each Mn^{4+} ion has six oxygen neighbors, and these MnO_6 octahedra are arranged in the structure to share edges and corners. Differences in the edge- and corner-sharing arrangements result in the various polymorphic structures.

If some of the Mn^{4+} ions are missing (cation vacancies), their missing positive charge has to be compensated by something else in the crystal structure. The Ruetschi model proposed that this charge balance is accomplished by the local presence of four protons. These protons would be bound to the neighboring oxide ions, forming a set of four OH^- ions. This local configuration is sometimes called a *Ruetschi defect*. There is very little volume change, as OH^- ions have essentially the same size as O^{2-} ions, and these species play the central role in determining the size of the crystal structure.

On the other hand, reduction of the MnO_2 occurs by the introduction of additional protons during discharge, as first proposed by Coleman [3], and does produce a volume change. The charge of these added mobile protons is balanced by a reduction in the charge of some of the manganese ions present from Mn^{4+} to Mn^{3+}. Mn^{3+} ions are larger than Mn^{4+} ions, and this change in volume during reduction has been observed experimentally.

The presence of protons (or OH^- ions) related to the manganese ion vacancies facilitates the transport of additional protons as the material is discharged. This is why these materials are very electrochemically reactive.

19.2.2 The Open Circuit Potential

The EMD is produced by oxidation of an aqueous solution of manganous sulfate at the positive electrode of an electrolytic cell. This means that the MnO_2 that is produced is in contact with water.

The phase relations, and the related ternary phase stability diagram, for the H–Mn–O system can be determined by use of available thermodynamic information [4, 5], as discussed in previous chapters. From this information it becomes obvious which neutral species reactions determine the potential ranges of the various phases present, and their values.

Following this approach, it is found that the lower end of the stability range of MnO_2 is at a potential that is 1.014 V vs. one atmosphere of H_2. The upper end is well above the potential at which oxygen evolves by the decomposition of water.

Under equilibrium conditions all oxides exist over a range of chemical composition, being more metal-rich at lower potentials, and more oxygen-rich at higher potentials. In the higher potential case, an increased oxygen content can result from either the presence of cation (Mn) vacancies or oxygen interstitials. In materials with the rutile, and related, structures that have close-packed oxygen lattices the excess energy involved in the formation of interstitial oxygens is much greater than that for the formation of cation vacancies. As a result, it is quite reasonable to assume that cation vacancies are present in the EMD MnO_2 that is formed at the positive electrode during electrolysis.

Due to the current that flows during the electrolytic process the potential of the MnO_2 that is formed is actually higher than the equilibrium potential for the decomposition of water. A number of other oxides with potentials above the stability range of water have been shown to oxidize water. Oxygen gas is evolved, and they become reduced by the insertion or protons. Therefore, it is quite reasonable to expect that EMD MnO_2 would have Mn vacancies, and that there would also be protons present, as discussed by Ruetschi [1, 2].

When such positive oxides oxidize water and absorb hydrogen as protons and electrons their potentials decrease to the oxidation limit of water, 1.23 V vs. H_2 at 25 °C. This is the value of the open circuit potential of MnO_2 electrodes in Zn/MnO_2 cells.

This water oxidation phenomenon that results in the insertion of protons into MnO_2 is different from the insertion of protons by the absorption of water into the crystal structure of materials that initially contain oxygen vacancies, originally discussed by Stotz and Wagner [6]. It has been shown that both mechanisms can be present in some materials [7, 8].

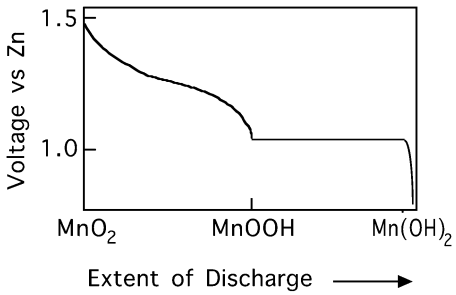

Fig. 19.1 Schematic discharge curve of Zn/MnO_2 cell

19.2.3 Variation of the Potential During Discharge

As mentioned above, this electrode operates by the addition of protons into its crystal structure. This is a single-phase insertion reaction, and therefore the potential varies with the composition, as discussed earlier.

If all of the initially present Mn^{4+} ions are converted to Mn^{3+} ions, the overall composition can be expressed as $HMnO_2$, or MnOOH.

It is also possible to introduce further protons, so that the composition moves in the direction of $Mn(OH)_2$. In this case, however, there is a significant change in the crystal structure, so that the mechanism involves the translation of a two-phase interface between MnOOH and $Mn(OH)_2$. This is analogous to the main reaction involved in the operation of the nickel electrode, as will be discussed later.

The sequence of these two types of reactions during discharge of a MnO_2 electrode is illustrated in Fig. 19.1.

The second, two-phase, reaction occurs at such a low cell voltage that the energy that is available is generally not used. Such cells are normally considered to only be useful down to about 1.2 V.

19.3 The "Nickel" Electrode

19.3.1 Introduction

The nickel electrode is widely used in battery technology, e.g., on the positive side of so-called Cd/Ni, Zn/Ni, Fe/Ni, H_2/Ni, and metal hydride/Ni cells, in some cases for a very long time. It has relatively rapid kinetics and exhibits unusually good cycling behavior. This is directly related to its mechanism of operation, which involves a solid state insertion reaction involving two ternary phases, $Ni(OH)_2$ and NiOOH, with no soluble product. While the attractive properties of this electrode have led to many investigations, there are still a number of aspects of its operation that are not fully understood. This chapter focuses primarily upon the microstructural mechanism of this two-phase insertion reaction and the thermodynamic features of the ternary Ni–O–H system that determine the observed potentials.

19.3.2 *Structural Aspects of the* $Ni(OH)_2$ *and* NiOOH *Phases*

The nanostructure of this electrode can be most simply described as a layer type configuration in which slabs of NiO_2 are separated by *galleries* in which various mobile guest species can reside. The structure of the NiO_2 layers consists of parallel sheets of hexagonally close-packed O^{2-} ions between which nickel ions occupy essentially all of the octahedral positions.

As will be described below, the mechanism of operation of this electrode involves the transition between $Ni(OH)_2$ and NiOOH upon oxidation, and the reverse upon reduction. Both of these phases are vario-stoichiometric (have ranges of stoichiometry). One can thus also describe their compositions in terms of the value of x in the general formula H_xNiO_2.

In the case of stoichiometric β $Ni(OH)_2$, the equilibrium crystal structure, which is isomorphous with *brucite*, $Mg(OH)_2$, has galleries that contain a proton concentration such that one can consider it as consisting of nickel-bonded layers of OH^- ions instead of O^{2-} ions. The nominal stoichiometry could thus be written as NiO_2H_2. Stoichiometric NiOOH has half as many protons in the galleries, and thus can be thought of as having an ordered mixture of O^{2-} and OH^- ions. Its nominal composition would then be H_1NiO_2.

When it is initially prepared, $Ni(OH)_2$ is often in the α modification, with a substantial amount of hydrogen-bonded water in the galleries. This structure is, however, not stable, and it gradually loses this water and converts to the equilibrium β $Ni(OH)_2$ structure, in which the galleries are free of water and contain only protons.

The equilibrium form of NiOOH, likewise called the β form, also has only protons in the galleries. However, there is also a γ modification of the NiOOH phase that contains water, as well as other species from the electrolyte, in the galleries. This γ modification forms at high charge rates or during prolonged overcharge in the alkali electrolyte. In both cases the potential is quite positive. It can also be formed by electrochemical oxidation of the α $Ni(OH)_2$ phase.

One can understand the transition of the β NiOOH to the γ modification at high potentials under overcharge conditions qualitatively in terms of the structural instability of the H_xNiO_2-type phase when the proton concentration is reduced substantially. Under those conditions, the bonding between adjacent slabs will be primarily of the relatively weak van der Waals type. This allows the entry of species from the electrolyte into the gallery space. This type of behavior is commonly found in other insertion reaction materials, such as TiS_2, mentioned in Chap. 9, if the interslab forces are weak and the electrolyte species are compatible.

The general relations between these various phases is generally described in terms of the scheme presented by Bode and co-workers [9].

A number of very good papers were published by the Delmas group in Bordeaux [10–14] that were aimed at the stabilization of the α $Ni(OH)_2$ phase by the presence of cobalt so that one might be able to cycle between the α $Ni(OH)_2$ and γ NiOOH

Table 19.1 Interslab distances for a number of phases related to the "nickel" electrode

Phase	Spacing (Å)
β-$Ni(OH)_2$	4.6
β-NiOOH	4.7
$NaNiO_2$	5.2
$Na_y(H_2O)_zNiO_2$	5.5
$Na_y(H_2O)_zCoO_2$	5.5
γ-$H_xNa_y(H_2O)_zNiO_2$	7.0
γ-$H_xK_y(H_2O)_zNiO_2$	7.0
γ′-$H_xNa_y(H_2O)_{2z}NiO_2$	9.9

phases. Since both of these phases have water, as well as other species, in the galleries, they have faster kinetics than the proton-conducting γ phases, although the potential is less positive. An important feature of their work has been the synthesis of sodium analogs by solid-state preparation methods and the use of solid-state ion-exchange techniques (*chimie douce*, or *soft chemistry*) to replace the sodium with other species [15].

The available information concerning the interslab spacing, the critical feature of the crystallographic structure of these phases in the nickel electrode, is presented in Table 19.1. It is readily seen that the crystallographic changes involved in the β $Ni(OH)_2$–β NiOOH reaction are very small, as they have almost the same value of interslab spacing. This is surely an important consideration in connection with the very good cycle life that is generally experienced with these electrodes. It can also be seen that the structural change involved in the a $Ni(OH)_2$–γ NiOOH transformation is somewhat larger. There are also differences in the slab stacking sequence in these various phases, but that factor will not be considered here.

Both the α and β versions of the $Ni(OH)_2$ phase are predominantly ionic, rather than electronic, conductors, and have a pale green color. The NiOOH phase, on the other hand, is a good electronic conductor, and both the β and γ versions are black.

19.3.3 Mechanism of Operation

The normal cycling reaction of commercial cells containing this electrode involves back and forth conversion between the β $Ni(OH)_2$ structure and the β NiOOH structure. It has been well established that these are separate, although vario-stoichiometric, phases, rather than end members of a continuous solid solution. The experimental evidence for this conclusion involves both x-ray measurements that show no gradual variation in lattice parameters with the extent of reaction [16], as well as similar IR observations [17] that indicate only changes in the amounts of the two separate phases as the electrode is charged or discharged.

Although the electrode potential when this two-phase structure is present is appreciably above the potential at which water is oxidized to form oxygen gas, as

recognized long ago by Conway [18], gaseous oxygen evolution cannot happen if the solid electrolyte $Ni(OH)_2$ separates the water from the electronic conductor NiOOH. Oxygen evolution can only occur when the electronically conducting NiOOH phase is present on the surface in contact with the aqueous electrolyte.

Therefore, as a first approximation, one can describe the microstructural changes occurring in the electrode in terms of the translation of the $Ni(OH)_2$/NiOOH interface. When the electrode is fully reduced, its structure consists of only $Ni(OH)_2$, whereas upon full oxidation, only NiOOH is present. This is shown schematically in Fig. 19.2. The crystallographic transition between the $Ni(OH)_2$ and NiOOH structures, with their different proton concentrations in the galleries, is shown schematically in Fig. 19.3.

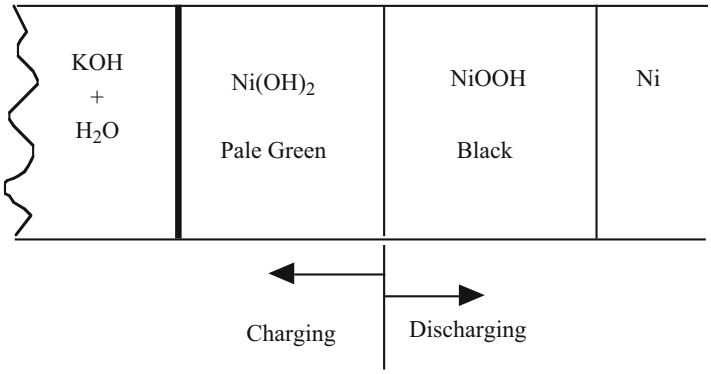

Fig. 19.2 Schematic drawing of the microstructure of the nickel electrode. The major phases present are $Ni(OH)_2$, which is a proton-conducting solid electrolyte, and NiOOH, a proton-conducting mixed conductor. The electrochemical reaction takes place by the translation of the $Ni(OH)_2$/NiOOH interface and the transport of protons through the $Ni(OH)_2$ phase

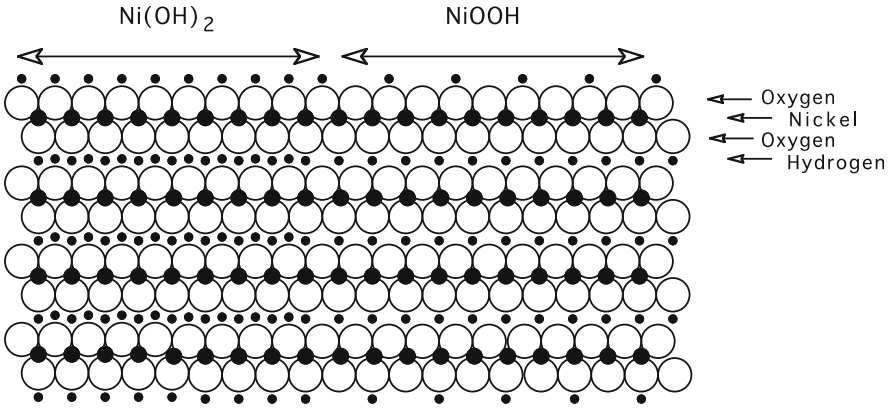

Fig. 19.3 Schematic drawing of the crystallographic transition between the $Ni(OH)_2$ and NiOOH structures, showing the step in the proton concentration in the galleries

It has long been known [19] that the NiOOH forms first at the interface between the $Ni(OH)_2$ and the underlying electronic conductor, rather than at the electrolyte/$Ni(OH)_2$ interface. Other authors (e.g., [20, 21]) have observed the motion of the color boundary during charge and discharge of such electrodes.

19.3.4 Relations Between Electrochemical and Structural Features

It is useful to consider the operation of this electrode in terms of the net reaction in which hydrogen is either added to or deleted from the layer structure. In the case of oxidation, this can be written as a neutral chemical reaction:

$$Ni(OH)_2 - {}^{1}\!/_{2}H_2 = NiOOH \tag{19.1}$$

However, in electrochemical cells this oxidation reaction takes place electrochemically, and since this normally involves an alkaline electrolyte, it is generally written in the electrochemical literature as

$$Ni(OH)_2 + OH^- = NiOOH + H_2O + e^- \tag{19.2}$$

However, the general rule is that electrochemical reactions take place at the boundary where there is a transition between ionic conduction and electronic conduction. Since $Ni(OH)_2$ is predominantly an ionic conductor (a solid electrolyte) the electrochemical reaction occurs at the $Ni(OH)_2$/NiOOH interface, where neither H_2O nor OH^- are present. The electrochemical reaction should therefore more properly be written as

$$Ni(OH)_2 - H^+ = NiOOH + e^- \tag{19.3}$$

In order for the reaction to proceed, the protons must be transported away from the interface through the galleries in the $Ni(OH)_2$ phase and into the electrolyte. However, in the alkaline aqueous electrolyte environment hydrogen is not present as either H^+ or H_2. Instead, hydrogen is transferred between the electrolyte and the $Ni(OH)_2$ phase by the interaction of neutral H_2O molecules and OH^- ions in the electrolyte with the H^+ ions at the electrolyte/$Ni(OH)_2$ interface. Thus the reaction at the electrolyte/$Ni(OH)_2$ interface must be electrically neutral and can be written as

$$OH^-{}_{(\text{electrolyte})} + H^+{}_{\left(Ni(OH)_2\right)} = H_2O \tag{19.4}$$

The equilibrium coulometric titration curve shows that under highly reducing conditions, when only the pale green $Ni(OH)_2$ phase is present throughout, there

is a relatively steep potential-composition dependence. However, the fact that this part of the titration curve is not vertical indicates that there is a range of composition in this phase. It was shown some time ago that up to about 0.25 electrons (and thus 0.25 protons) per mole can be deleted from the $Ni(OH)_2$ phase before the onset of the two-phase $Ni(OH)_2$/NiOOH equilibrium [21]. Translated to the crystallographic picture, this means that the proton concentration in the phase nominally called $Ni(OH)_2$ can deviate significantly from the stoichiometric value, up to a proton vacancy fraction of some 12.5 %. The proton-deficient composition limit for the $Ni(OH)_2$ phase can thus be expressed as $H_{(1.75}NiO_2)$.

When both phases are present, there is a relatively long constant-potential plateau in the limit of negligible current density. This extends from the proton deficient concentration limit in the $Ni(OH)_2$ phase ($H_{(1.75}NiO_{2)}$) to the maximum proton concentration in the NiOOH phase. According to Barnard et al. [21] this is when about 0.75 electrons (or protons) per mole are deleted from the electrode. This is equivalent to a composition of $H_{1.25}NiO_2$. Under more oxidizing conditions, when further protons are deleted, the potential of the NiOOH phase becomes more positive.

The apparent length of the constant potential two-phase plateau that is observed experimentally depends upon when the NiOOH phase reaches the electrolyte/electrode interface, and thus upon the thickness of the $Ni(OH)_2$ phase and the geometrical shape of the $Ni(OH)_2$/NiOOH interface. The morphology of this interface, which is often not flat [22], is dependent upon several factors. As will be discussed subsequently, a flat interface is inherently unstable during the oxidation reaction. On the other hand, the interface will tend toward a smooth shape when it translates in the reduction direction. In both cases, it will be shown that the current density is a critical parameter.

Under more oxidizing conditions, when only the NiOOH phase is present, the electrode is black and electronically conducting. This phase has wide ranges of both composition and potential. As mentioned above, the upper limit of proton concentration has been found to be approximately $H_{1.25}NiO_2$ for the β modification. Upon further oxidation in the NiOOH single-phase regime the gallery proton concentration is reduced. It is generally found that the proton concentration can be substantially lower for the γ modification than in the β case. These can thus be far from the nominal composition of NiOOH.

19.3.5 Self-Discharge

Since the NiOOH phase is a good mixed-conductor, with a high mobility of both ionic and electronic species, equilibrium with the adjacent electrolyte is readily attained. In the absence of current through the external circuit, there will be a chemical reaction at the NiOOH surface with water in the electrolyte that results in the addition of hydrogen to the electrode. This causes a shift in the direction of a

less positive potential. This increase in the hydrogen content and decrease of the potential thus results effectively in a gradual self-discharge of the electrode.

The electrochemical literature generally assumes that this self-discharge reaction involves the generation of oxygen, since the potential of the electrode is more positive than that necessary for the evolution of oxygen by the decomposition of water, as mentioned above.

There are two possible oxygen evolution reactions involving species in the electrolyte:

$$2\mathrm{NiOOH} + \mathrm{H_2O} = 2\mathrm{Ni(OH)_2} + {}^{1}\!/\!_{2}\mathrm{O_2} \tag{19.5}$$

which can also be written as

$$\mathrm{H_2O} = {}^{1}\!/\!_{2}\mathrm{O_2}(\text{into electrolyte or gas}) + \mathrm{H_2}(\text{into electrode}) \tag{19.6}$$

and

$$2\mathrm{OH^-} = \mathrm{H_2O} + {}^{1}\!/\!_{2}\mathrm{O_2} + 2e^- \tag{19.7}$$

However, the latter does not provide any hydrogen to the electrode, and thus cannot contribute to self-discharge. Instead, it is the electrochemical oxygen evolution reaction, involving passage of current through the outer circuit, as mentioned later.

The rate of the self-discharge reaction can be simply measured for any value of electrode potential in the single-phase NiOOH regime, where the potential is state-of-charge dependent by using a potentiostat to hold the potential at a constant value, and measuring the anodic current through the external circuit that is required to maintain that value of the potential (and thus also the corresponding proton concentration in the electrode). This is the opposite of the self-discharge process, and can be written as

$$2\mathrm{Ni(OH)_2} + \mathrm{OH^-} = 2\mathrm{NiOOH} + \mathrm{H_2O} + e^- \tag{19.8}$$

Measurements of the self-discharge current as a function of potential in the NiOOH regime for the case of electrodes produced by two different commercial manufacturers are shown in Fig. 19.4. The differences between the two curves are not important, as they are related to differences between the microstructures of the two electrodes.

If anodic current is passed through the NiOOH electrode, part will be used to counteract the self-discharge mentioned above. If the magnitude of the current is greater than the self-discharge current, additional protons will be removed from the electrode's crystal structure, making the potential more positive. This results in an increased rate of self-discharge. Thus a steady state will evolve in which the applied current will be just balanced by the rate of self-discharge and the proton concentration in the galleries will reach a new steady (lower) value.

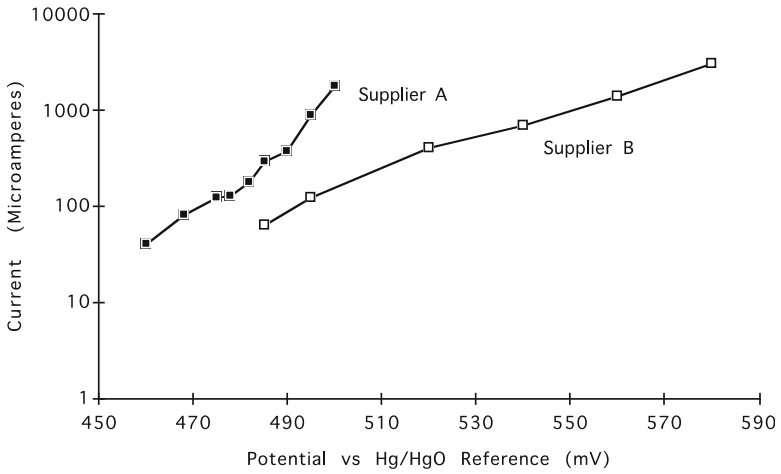

Fig. 19.4 Self-discharge current as a function of potential in the NiOOH regime measured on electrodes produced by two different commercial manufacturers

19.3.6 Overcharge

If the applied current density exceeds that which can be accommodated by the kinetics of the compositional change and the self-discharge process, another mechanism must come into play. This is the direct generation of oxygen gas at the electrolyte/NiOOH interface by the decomposition of water in the electrolyte. This can be described by the reaction

$$2\,OH^- = H_2O + {}^1\!/_2 O_2 + 2e^- \tag{19.9}$$

in which the electrons go into the current collector

The relationship between the potential of the "nickel" electrode and the amount of hydrogen that is deleted when it is charged (oxidized) is shown schematically in Fig. 19.5.

19.3.7 Relation to Thermodynamic Information

The available thermodynamic data relating to the various phases in the Ni–O–H system can be used to produce a ternary phase stability diagram. From this information, one can also readily calculate the potentials of the various possible stable phase combinations. This general methodology [23–26] has been used with great success to understand the stability windows of a number of electrolytes, as well as the potential-composition behavior of many electrode materials in lithium, sodium, oxide, and other systems.

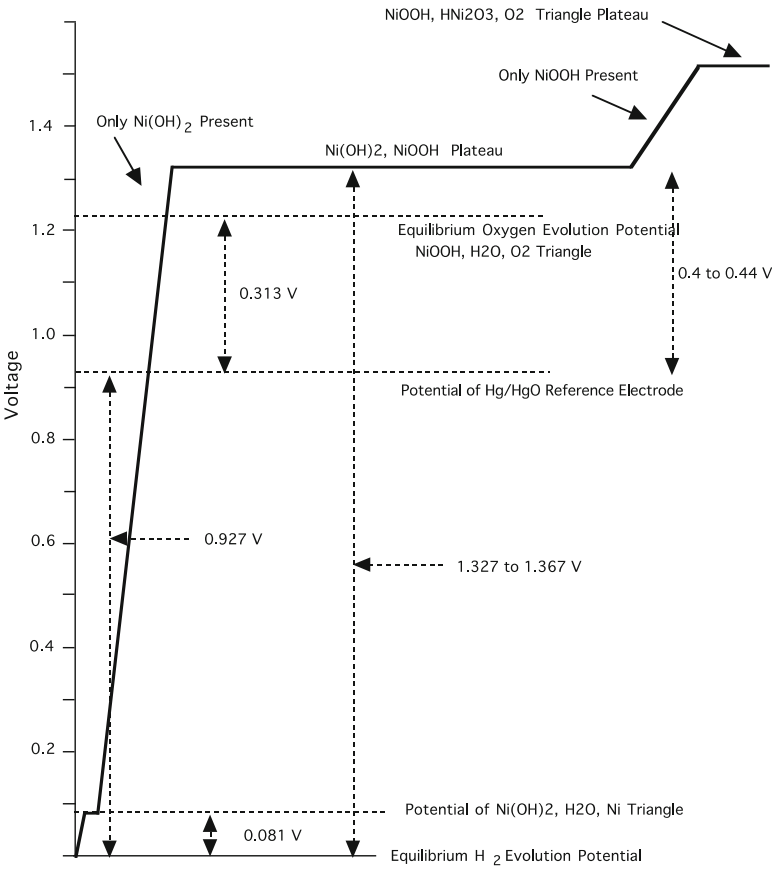

Fig. 19.5 Variation of the potential as hydrogen is removed from the nickel electrode during oxidation when the cell is being charged

With this information, the microstructural model discussed above, and the available information about the stoichiometric ranges of the important phases, one should be able to explain the observed electrochemical behavior of the nickel electrode.

Unfortunately, reliable thermodynamic information for this system is rather scarce. The data that have been used are included in Table 19.2, taken mostly from the compilation in [27]. Unfortunately, no recognition was given to the question of stoichiometry or the ordered/disorder state of crystal perfection, or even to the differences between the α and β structures of $Ni(OH)_2$ and the β and γ structures of NiOOH. Therefore, the calculated potentials can only be considered semiquantitative at present.

The results of these calculations are shown in the partial ternary phase stability diagram of Fig. 19.6, in which all phases are assumed to have their

Table 19.2 Thermodynamic data

Phase	ΔG_f° (25 °C)
NiO	−211.5
NiOOH	−329.4
$Ni(OH)_2$	−458.6
H_2O	−237.14

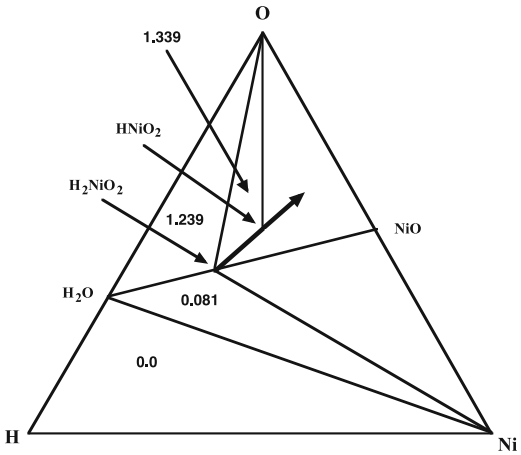

Fig. 19.6 Partial Gibbs triangle. The main charge-discharge reaction takes place along the thick line at 1.339 V vs. H_2. The overall composition moves along that line upon further charging

nominal compositions. The two-phase tie lines and three-phase triangles indicate the phases that are stable in the presence of each other at ambient temperatures. Also shown are the potentials of the various relevant three-phase equilibria versus the hydrogen evolution potential at one atmosphere. The composition of the electrode during operation on the main plateau follows along the heavy line that points toward the hydrogen corner of the diagram and lies on the edge of the triangle in which all compositions have a potential of 1.339 V vs. hydrogen.

Parts of this figure are incomplete, for the data available did not indicate what happens when additional hydrogen is removed from $HNiO_2$ and the potential exceeds 1.339 V at the time that it was first written [28]. It was obvious, of course, that the composition follows further along the arrow, but the species at the corners of the sub-triangle that has the observed higher potential could not be identified. Subsequent information, that led to an explanation of the so-called *memory effect*, is discussed later in this chapter.

One important question is whether there is a stable tie line between NiOOH and H_2O. The alternative is a tie line between $Ni(OH)_2$ and oxygen. Only one of these can be stable, as tie lines cannot cross. The Gibbs free energy change involved in the determining reaction can be calculated as

$$2\mathrm{NiOOH} + \mathrm{H_2O} = 2\mathrm{Ni(OH)_2} + {}^1\!/_2\mathrm{O_2} \qquad (19.10)$$

This is found to be −21.26 kJ at 25 °C, which means that the NiOOH–H_2O tie line is not stable, and that there is a stable three-phase equilibrium involving $Ni(OH)_2$, NiOOH, and oxygen. A situation in which both $Ni(OH)_2$ and NiOOH are in contact with water can only be metastable.

It is possible to calculate the potential of the $Ni(OH)_2$, NiOOH, O_2 triangle relative to the one atmosphere hydrogen evolution potential from the reaction

$$^1/_2H_2 + NiOOH = Ni(OH)_2 \tag{19.11}$$

that is the primary reaction of the nickel electrode, as discussed above, since this reaction occurs along one of the sides of this three-phase equilibrium triangle. From the data in Table 19.2 it can be determined that the Gibbs free energy change ΔG_r° accompanying this reaction is −129.2 kJ per mol. From the relation

$$\Delta G_r{}^0 = -zFE \tag{19.12}$$

since z is unity for this reaction, the equilibrium potential is 1.34 V positive of the hydrogen evolution potential.

Since the potential of a Hg/HgO reference electrode is 0.93 V positive of the reversible hydrogen evolution potential (RHE), this calculation predicts that the equilibrium value of the two-phase constant potential plateau for the main reaction of the nickel electrode should occur at about 0.41 V positive of the *Hg/HgO* reference. This is also about 0.11 V more positive than the equilibrium potential of oxygen evolution from water.

This result can be compared with the experimental information from Barnard et al. [21] on the potentials of both the *activated* (highly disordered) and *deactivated* (more highly ordered) β $Ni(OH)_2$–β NiOOH reaction. Their data fell in the range 0.44–0.47 V positive of the *Hg/HgO* electrode potential. They found the comparable values for the a $Ni(OH)_2$–γ NiOOH reaction to be in the range 0.39–0.44 V relative to the Hg/HgO reference. Despite the lack of definition of the structures to which the thermodynamic data relate, this should be considered to be a quite good correlation.

Further oxidation causes the electrode composition to move along the arrow further away from the hydrogen corner of the ternary diagram, and leads to an electrode structure in which the $Ni(OH)_2$ phase is no longer stable, as is found experimentally. The potential moves to more positive values as the stoichiometry of the NiOOH phase changes, and if no other reaction interferes, should eventually arrive at another, higher, plateau in which the lower proton concentration limit NiOOH is in equilibrium with some other phase or phases.

Another complicating fact is that electrolyte enters the β NiOOH at high potentials, converting it to the γ modification. As mentioned earlier, the water-containing α $Ni(OH)_2$ and γ NiOOH phases are not stable, and during normal cycling are gradually converted to the corresponding β phases that have only protons in their galleries. When these metastable phases are present the electrode

potential of the reaction plateau is less positive, as is characteristic of insertion structures with larger interslab spacings. Correspondingly, the apparent capacity of the electrode prior to rapid oxygen evolution is greater. These several factors are discussed further in the next chapter.

19.4 Cause of the Memory Effect in "Nickel" Electrodes

19.4.1 Introduction

It is often found that batteries with nickel positive electrodes, e.g., Cd/Ni, Hydride/Ni, Zn/Ni, Fe/Ni, and H_2/Ni cells, have a so-called *memory effect*, in which the available capacity apparently decreases if they are used under conditions in which they are repeatedly only partially discharged before recharging. In many cases these batteries are kept connected to their chargers for long periods of time. It is also widely known that this problem can be "cured" by subjecting them to a slow, deep discharge.

The phenomena that take place in such electrodes have been studied by many investigators over many years, but no rational and consistent explanation of the *memory effect* related to nickel electrodes emerged until recently. Although it has important implications for the practical use of such cells, some of the major reviews in this area don't even mention this problem, and others give it little attention and/or no explanation.

In studying this apparent loss of capacity, a number of investigators have shown that a second plateau appears at a lower potential during discharge of nickel electrodes [29–45]. Importantly, it is found that under low current conditions the total length of the two plateaus remains constant. As the capacity on the lower one, sometimes called *residual capacity*, becomes greater, the capacity of the higher one shrinks. The relative lengths of the two plateaus vary with the conditions of prior charging. This is shown schematically in Fig. 19.7.

Since the capacity of the lower plateau is at about 0.78 V positive of the reversible hydrogen electrode potential, it is generally not useful for most of the applications for which nickel electrode batteries are employed. The user does not see this capacity, but instead, sees only the dwindling capacity on the upper plateau upon discharge. Thus it is quite obvious that the appearance of this lower plateau and reduction in the length of the upper plateau is an important component of the memory effect.

It is also found that this lower plateau and the memory effect both disappear if the cell is deeply discharged. Thus the existence of the lower plateau, and its disappearance, are both obviously related to the *curing* of the memory effect.

These phenomena can now be explained on the basis of available thermodynamic and structural information by using the ternary Gibbs phase stability diagram for the H–Ni–O system as a thinking tool [46, 47].

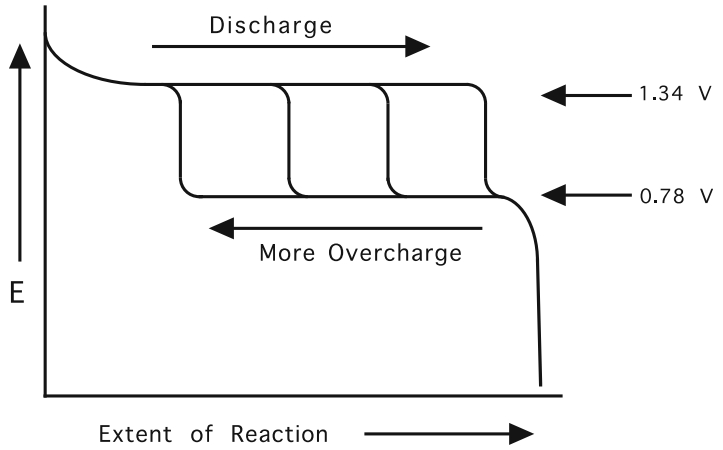

Fig. 19.7 Schematic representation of the two discharge plateaus. With increasing overcharge the length of the upper one decreases and the lower one increases

19.4.2 Mechanistic Features of the Operation of the "Nickel" Electrode

The microscopic mechanism of the basic operation of these electrodes was discussed earlier in this chapter. However, it is important for this discussion, and will be briefly reviewed here. It involves an insertion reaction that results in the translation of a two-phase interface between H_2NiO_2 and $HNiO_2$, both of which are vario-stoichiometric (have ranges of stoichiometry). The H_2NiO_2 is in contact with the alkaline electrolyte, and the $HNiO_2$ is in contact with the metallic current collector. The outer layer of the H_2NiO_2 phase is pale green and is predominantly an ionic conductor, allowing the transport of protons to and from the two-phase $H_2NiO_2/HNiO_2$ boundary. $HNiO_2$ is a good electronic conductor, and is black. The electrochemical reaction takes place at that ionic/electronic two-phase interface. This boundary is displaced as the reaction proceeds, and the motion of the color boundary has been experimentally observed. When the electrode is fully reduced, its structure consists of only H_2NiO_2, whereas oxidation causes the interface to translate in the opposite direction until only $HNiO_2$ is present. Although these are both ternary phases, the only compositional change involves the amount of hydrogen present, and the structure of the host "NiO_2" does not change. Thus this is a pseudo-binary reaction, although it takes place in a ternary system, and the potential is independent of the overall composition, i.e., the state of charge.

Once the H_2NiO_2 has been completely consumed, and the $HNiO_2$ phase comes into contact with the aqueous electrolyte it is possible to obtain further oxidation. This involves a change in the hydrogen content of the $HNiO_2$ phase. The variation of the composition of this single phase results in an increase in the potential from this two-phase plateau to higher values, as is expected from the Gibbs phase rule.

After the low-hydrogen limit of the composition of the $HNiO_2$ phase is reached, further oxidation can still take place. Another potential plateau is observed, and oxygen evolution occurs. This is often called *overcharging*, and obviously involves another process.

A number of authors have shown that the length of the lower plateau observed upon discharging is a function of the amount of the γ NiOOH phase formed during overcharging [38]. However, other authors [12] have shown that it is possible to prevent the formation of the γ phase during overcharging by using a dilute electrolyte. Yet the lower discharge potential plateau still appears. There is also evidence that the γ phase can disappear upon extensive overcharging, but the lower discharge plateau is still observed [38].

Neutron diffraction studies [43], which see only crystalline structures, showed a gradual transition between the γ and β NiOOH structures upon discharge, with no discontinuity at the transition between the upper and lower discharge plateaus. There was no evidence of a change in the compositions of either of the two phases, just a variation in their amounts, which changed continuously along both discharge plateaus. These authors attributed the presence of the lower plateau to undefined "technical parameters."

Several other authors have explained the presence of the lower discharge plateau in terms of the formation of some type of barrier layer [30, 36], and there is evidence for the formation of β H_2NiO_2, which is not electronically conducting, on the lower plateau [41]. This can, of course, be interpreted as a barrier.

These studies all seem to assume that the oxygen that is formed during operation upon the upper plateau during charging comes only from decomposition of the aqueous electrolyte. However, something else is obviously happening that leads to the formation of the lower plateau that is observed upon discharge. It must also relate to a change in the amounts, compositions or structure of the solid phase, or phases, present.

Although the electrochemical behavior of the nickel electrode upon the lower potential plateau can be understood in terms of a pseudo-binary insertion/extraction hydrogen reaction, the evolution of oxygen and the formation of the second discharge plateau indicate that the assumption that the oxygen comes from (only) the electrolysis of the aqueous electrolyte during overcharge cannot be correct. In order to understand this behavior, recognition must be given to the fact that the evolution of oxygen indicates that at this potential this electrode should be treated in terms of the ternary H–Ni–O system, rather than as a simple binary phase reaction.

Use of the Gibbs triangle as a *thinking tool* to understand the basic reactions in the H–Ni–O system has been discussed in several places [48–50]. The major features of the lower-potential portion of this system can be readily determined from available thermodynamic information. A major part of the Gibbs phase stability triangle for this system is again shown in Fig. 19.8, copied from the discussion earlier in this chapter.

Since the two phases H_2NiO_2 and $HNiO_2$ are on a tie line that points to the hydrogen corner, neither hydrogen insertion nor deletion involve any change in the Ni/O_2 ratio, and this can be considered to be a pseudo-binary reaction. The tie line between those two phases is one side of a triangle that has pure oxygen at its other corner. This means that both of these phases are stable in oxygen, as is well known.

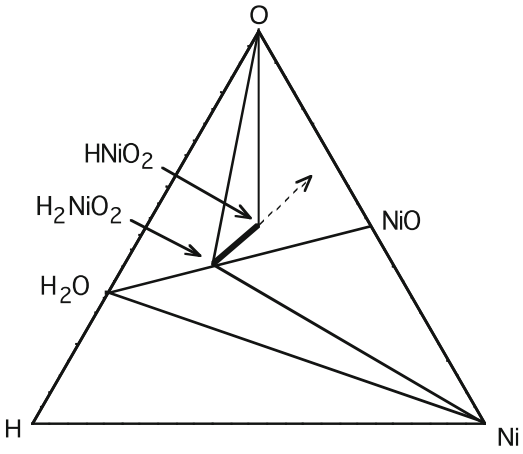

Fig. 19.8 Partial Gibbs triangle. The main charge-discharge reaction takes place along the *thick line*. The overall composition moves along the *dashed line* upon further charging

As the result of the Gibbs phase rule, movement of the overall composition along this tie line occurs at a constant potential plateau. It was shown earlier that the potential of this plateau is 1.34 V versus pure hydrogen at 25 °C.

Thus the equilibrium electrode potential of the basic H_2NiO_2–$HNiO_2$ reaction is not only composition-independent, but also more positive than the potential of the decomposition of water, as is experimentally observed. Also, because the H_2NiO_2 that is between the $HNiO_2$ and the water is a solid electrolyte, there is little or no oxygen evolution.

As additional hydrogen is removed the potential moves up the curve where only $HNiO_2$ is present. When the overall composition exceeds the stability range of that phase it moves further from the hydrogen corner and enters another region in the phase diagram, as indicated by the dashed line in Fig. 19.2.

19.4.3 Overcharging Phenomena

The potential then moves along the upper charging (or overcharging) plateau. Since all of the area within a Gibbs triangle must be divided into sub-triangles, the overall composition must be moving into a new sub-triangle. One corner of this new triangle must be $HNiO_2$, and another must be oxygen. This is consistent with the observation that oxygen is evolved at this higher charging potential. The question is then, what is the composition of the phase that is at the third corner?

If gaseous oxygen is evolved from the electrode, not just from decomposition of the water, the third-corner composition must be below (i.e., have less oxygen) than all compositions along the dashed line.

One possibility might be the phase Ni_3O_4, another could be NiO. However, neither of these phases, which readily crystallize, has been observed. There must be another phase with a reduced ratio of oxygen to nickel.

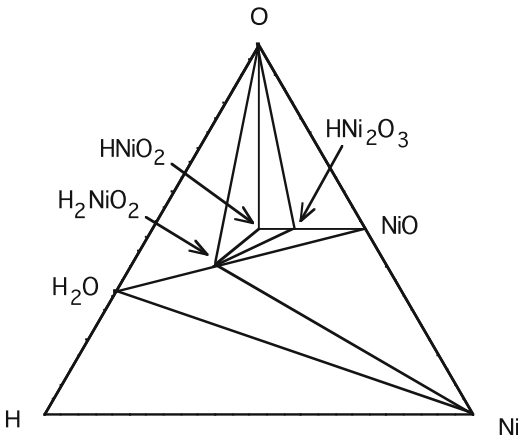

Fig. 19.9 Gibbs triangle showing the presence of the HNi_2O_3 phase

Although evidently not generally recognized by workers interested in the nickel electrode, it has been found [51, 52] that a phase with a composition close to HNi_2O_3 can be formed under conditions comparable to those during charging the electrode on the upper voltage plateau. This phase can form as an amorphous product during the oxidation of $HNiO_2$. It's crystal structure and composition were determined after hydrothermal crystallization. In addition, the mean nickel oxidation state was found by active oxygen analysis to be only 2.65.

The composition HNi_2O_3 lies on a line connecting $HNiO_2$ and NiO. This would then lead to a sub-triangle as shown in Fig. 19.9, which meets the requirement that there be another phase in equilibrium with both $HNiO_2$ and oxygen that has a reduced ratio of oxygen to nickel.

The gradual formation of amorphous HNi_2O_3 during oxygen evolution upon the upper overcharging plateau, and its influence upon behavior during discharge, is the key element in the memory effect puzzle.

As overcharge continues, oxygen is evolved, and more and more of the HNi_2O_3 phase forms. Thus the overall composition of the solid gradually shifts along the line connecting $HNiO_2$ and HNi_2O_3.

Upon discharge, the overall composition moves in the direction of the hydrogen corner of the Gibbs triangle. This is indicated by the dashed line in Fig. 19.10.

It is seen that the HNi_2O_3 portion of the total solid moves into a different sub-triangle that has H_2NiO_2, HNi_2O_3 and NiO at its corners. From the available thermodynamic data one can calculate that the potential in this sub-triangle is 0.78 V versus hydrogen. That is essentially the same as experimentally found for the lower discharge plateau. The larger the amount of HNi_2O_3 that has been formed during overcharging, the longer the corresponding lower discharge plateau will be. The upper discharge plateau becomes correspondingly shorter.

After traversing this triangle, the overall composition of what had been HNi_2O_3 moves into another sub-triangle that has H_2NiO_2, NiO, and Ni at its corners. The HNi_2O_3 disappears, and the major product is H_2NiO_2. The potential in this sub-triangle can be calculated to be 0.19 V versus hydrogen.

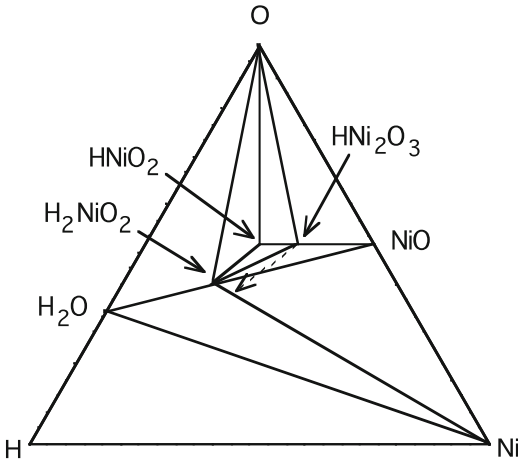

Fig. 19.10 Composition path during the discharge of the HNi_2O_3 formed during overcharge

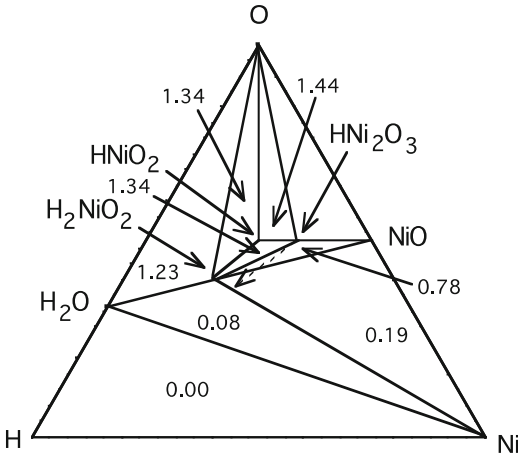

Fig. 19.11 Calculated values of the potential in the various sub-triangles in the H–Ni–O ternary system versus hydrogen. It is seen how the composition path during discharge of HNi_2O_3 leads to the observation of the lower discharge plateau at about 0.78 V, and the disappearance of that phase when the potential moves to a much lower value

If the electrode is now recharged, its potential does not go back up to the 0.8 V plateau, since HNi_2O_3 is no longer present, but goes to the potential for the oxidation of its major component, H_2NiO_2, The overall composition again moves away from the hydrogen corner, and the H_2NiO_2 loses hydrogen and gets converted to $HNiO_2$. This is the standard charging cycle low potential plateau. This also means that the lower reduction plateau is no longer active, for the HNi_2O_3 has disappeared, and the *memory effect* has been *cured*.

The calculated potentials in the various sub-triangles of the H–Ni–O system are shown in Fig. 19.11.

The reactions in the H–Ni–O system obviously have very rapid kinetics, for this electrode can be both charged and discharged at high rates. Therefore, it is quite reasonable to expect the phases present to be at or near their equilibrium amounts and compositions. This is indicated by the very good correlation between experimental results and the information obtained by the use of ternary phase stability diagrams based upon the available thermodynamic data.

19.4.3.1 Conclusions

The basic mechanisms that are involved in causing the memory effect have been identified. The key element is the formation of an amorphous HNi_2O_3 phase upon overcharging into the potential range where oxygen is evolved. Upon subsequent reduction, the presence of this phase produces the potential plateau at about 0.8 V versus hydrogen, reducing the available capacity at the normal higher reduction potential. The more the overcharge, the more HNi_2O_3 that is formed, and the longer the lower plateau. If the electrode undergoes further reduction this phase disappears, and the potential drops to a much lower value. Subsequent charging of the electrode brings the composition back to the initial state, and the *memory effect is cured*.

This model provides an understanding of the main features of the memory effect, and also explains the several confusing and apparently contradictory observations in the literature. It is expected that further experimental work will address this matter. Additional confirmation of the presence of HNi_2O_3 in the microstructures of overcharged electrodes would be especially useful.

The implication from this mechanism is that the major reason for the memory effect, a decrease in the capacity at the normal discharge potential, is related to extensive overcharging, rather than to the use of shallow discharge cycles.

References

1. Ruetschi P (1984) Cation-Vacancy Model for MnO_2. J Electrochem Soc 131:2737
2. Ruetschi P, Giovanoli R (1988) J Electrochem Soc 135:2663
3. Coleman JJ (1946) Trans Electrochem Soc 90:545
4. Barin (1995) Thermochemical Data of Pure Substances, 3rd edn. VCH, ISBN 9783527619825
5. Pourbaix M (1966) Atlas of Electrochemical Equilibria. Pergamon, Oxford
6. Stotz S, Wagner C (1966) Ber Bunsenges Physik Chem 70: 781
7. Netz A, Chu WF, Thangadurai V, Huggins RA, Weppner W (1999) Ionics 5:426
8. Huggins RA (2006) J Power Sources 153:365
9. Bode H, Dehmelt K, Witte J (1966) Electrochim Acta 11:1079
10. Oliva P et al (1982) J Power Sources 8:229
11. Faure C et al (1991) J Power Sources 35:249
12. Faure C, Delmas C, Willmann P (1991) J Power Sources 35:263
13. Faure C, Delmas C, Fouassier M (1991) J Power Sources 35:279

14. Delmas C (1991) In: Nazri GA, Shriver DF, Huggins RA, Balkanski M (eds) Solid State Ionics II. Materials Research Society, p 335
15. Delmas C et al (1988) Solid State Ionics 28–30:1132
16. Briggs GWD, Jones E, Wynne-Jones WFK (1955) Trans Faraday Soc 51:394
17. Kober FP (1965) J Electrochem Soc 112:1064
18. Conway BE, Bourgault PL (1959) Can J Chem 37:292
19. Kuchinskii EM, Erschler BV (1940) J Phys Chem 14:985
20. Briggs GWD, Fleischmann M (1971) Trans Faraday Soc 67:2397
21. Barnard R, Randell CF, Tye FL (1980) J Appl Electrochem 10:109
22. Crocker RW, Muller RH (1992) Presented at the Meeting of the Electrochemical Society, Toronto
23. Huggins RA (1979) In: Vashishta PP, Mundy JN, Shenoy GK (ed) Fast Ion Transport in Solids. North-Holland, p 53
24. Weppner W, Huggins RA (1980) Solid State Ionics 1:3
25. Godshall NA, Raistrick ID, Huggins RA (1980) Mater Res Bull 15:561
26. Godshall NA, Raistrick ID, Huggins RA (1984) J Electrochem Soc 131:543
27. Balej J, Divisek J (1992) Presented at the Meeting of the Bunsengesellschaft, Wien.
28. Huggins RA, Wohlfahrt-Mehrens M, Jörissen L (1993) Presented at Symposium on Intercalation Chemistry and Intercalation Electrodes. Meeting of the Electrochemical Society in Hawaii, Spring 1993
29. Milner PC, Thomas UB (1967) In: Tobias CW (ed) Advances in Electrochemistry and Electrochemical Engineering. p 1
30. Barnard R, Crickmore GT, Lee JA, Tye FL (1980) J Appl Electrochem 10:61
31. Klapste B, Mickja K, Mrha J, Vondrak J (1982) J Power Sources 8:351
32. Zimmerman AH, Effa PK (1984) J Electrochem Soc 131:709
33. Lim HS, Verzwyvelt SA (1988) J Power Sources 22:213
34. Vaidyanathan H (1988) J Power Sources 22:221
35. McBreen J (1990) Mod Aspect Electrochem 21:29
36. Zimmerman AH (1990) In: Corrigan DA, Zimmerman AH (ed) Nickel Hydroxide Electrode. Electrochem Soc Proc 90-4: 311
37. Zimmerman AH (1994) Proc IECEC 4:63
38. Wilde P (1996) PhD Thesis. University of Ulm, Germany
39. Sac-Epee N, Palacín MR, Beaudoin B, Delahaye-Vidal A, Jamin T, Chabre Y, Tarascon J-M (1997) J Electrochem Soc 144:3896
40. Sac-Epee N, Palacìn MR, Delahaye-Vidal A, Chabre Y, Tarâscon J-M (1998) J Electrochem Soc 145:1434
41. Leger C, Tessier C, Ménétrier M, Denage C, Delmas C (1999) J Electrochem Soc 146:924
42. Fourgeot F, Deabate S, Henn F, Costa M (2000) Ionics 6:364
43. Deabate S, Fourgeot F, Henn F (2000) Ionics 6:415
44. Barde F, Palacin MR, Chabre Y, Isnard O, Tarascon J-M (2004) Chem Mater 16:3936
45. Huggins RA (2006) Solid State Ionics 177:2643
46. Huggins RA (2007) J Power Sources 165:640
47. Huggins RA, Wohlfahrt-Mehrens M, Jörissen L (1992) Presented at Meeting of the Electrochemical Society, Hawaii
48. Huggins RA, Wohlfahrt-Mehrens M, Jörissen L (1993) In: Nazri GA, Tarascon JM, Armand (eds) Solid State Ionics III. Mater Res Soc Proc 293: 57
49. Huggins RA, Prinz H, Wohlfahrt-Mehrens M, Jörissen L, Witschel W (1994) Solid State Ionics. 70/71: 417
50. Greaves C, Thomas MA, Turner M (1983) Power Source 9:163
51. Greaves C, Malsbury AM, Thomas MA (1986) Solid State Ionics. 18/19: 763
52. Malsbury AM, Greaves C (1987) J Solid State Chem 71:418